Journal of Electroanalytical Chemistry 936 (2023) 117376

Contents lists available at ScienceDirect

Journal of Electroanalytical Chemistry

journal homepage: www.elsevier.com/locate/jelechem

Electrochemical evaluation of $Sr_2Fe_{1.5}Mo_{0.5}O_{6-\delta}/Ce_{0.9}Gd_{0.1}O_{1.95}$ cathode of SOFCs by EIS and DRT analysis

Arsalan Zare [a], Hirad Salari [a], Alireza Babaei [a,*], Hamid Abdoli [b,*], Hamed Aslannejad [c]

[a] School of Metallurgy and Materials Engineering, College of Engineering, University of Tehran, Tehran, Iran
[b] Renewable Energy Research Department, Niroo Research Institute (NRI), Tehran, Iran
[c] Copernicus Institute of Sustainable Development, Utrecht University, 3584 CS Utrecht, the Netherlands

ARTICLE INFO

Keywords:
Solid oxide fuel cell
EIS
DRT
SFM/GDC
Gerischer

ABSTRACT

Employing potent advanced materials to perform as the cathode of SOFC requires a profound investigation on the material's electrochemical response within the oxygen reduction reaction. Accordingly, in this research, electrochemical characteristics of $Sr_2Fe_{1.5}Mo_{0.5}O_{6-\delta}/Gd_{0.1}Ce_{0.9}O_{1.5}$ (SFM/GDC) air electrode was studied using electrochemical impedance spectroscopy (EIS) and distribution of relaxation time (DRT) technique. SFM/GDC composite electrode sintered at 1050 °C shows the lowest polarization resistance of 0.23 Ω.cm^2 at 800 °C. Three DRT peaks determined, and an $LR_\Omega(QR_H)G$ equivalent circuit is proposed for the EIS response, in which the Gerischer element was related to the low-frequency part. Two of the peaks indicated by DRT were associated to the Gerischer response, which reveals simultaneous occurrence of oxygen surface reaction and diffusion sub-processes during ORR. By temperature rising from 650 °C to 800 °C, Gerischer resistance (R_G) reduces by 91%. Introduction of Pd nanoparticles into the electrode reduces the R_G by 48% and 10% at 650 °C and 800 °C, respectively. The results demonstrate that at the intermediate temperature range, the SFM/GDC composite electrode requires improvement by surface decoration due to its insufficient surface exchange kinetics; however, significantly improved surface exchange kinetics is observed at higher temperature range without any surface modification.

1. Introduction

Study of the electrochemical behavior of electrode materials is of great importance to utilize them in solid oxide cells (SOCs) as one of the most promising energy conversion systems [1–3]. Introduction of double perovskite (DP) and the Ruddlesden-Popper (RP) structures established new classes of electrode materials that exhibited superior performance compared to simple perovskite materials [4]. Recently, strontium ferrite-molybdenum with double perovskite structure has been introduced with notable electrical conductivity in both oxidizing and reducing atmospheres, makes it suitable to be used as both air and fuel electrodes [5–9]. It was reported that manipulating the B site cations ratio in $Sr_2Fe_{1.5}Mo_{0.5}O_{6-\delta}$ (SFM) leads to the emergence of electronic defects and oxygen vacancies in the material's structure, which are the prerequisites of mixed ionic and electronic conductor (MIEC) materials. Also, its electrical conductivity increases by temperature especially above 630 °C due to the change in the electronic state of Fe and Mo from Fe^{2+}/Mo^{6+} to Fe^{3+}/Mo^{5+} [7,10,11]. However, it is repeatedly reported that SFM electrode material suffers from the presence of insulator $SrMoO_4$ phase [9,12].

SFM and SFM-based composite electrodes have been studied to evaluate their feasibility for use as air electrode of SOFC. For the first time, Liu et al. [7] reported that the electrode polarization resistance of SFM air electrode on LSGM electrolyte is 0.66, 0.24 and 0.10 Ω.cm^2 at 750, 800 and 850 °C, respectively. Afterwards, oxide ion conductors such as Sm- and Gd-doped CeO_2 (SDC and GDC, respectively) were utilized to make SFM-based composite cathodes in order to improve the electrochemical activity of the electrode by the extension of active sites [13,14]. Dai et al. [13] studied the electrochemical response of SFM/SDC composite cathode and obtained the lowest polarization resistance in the presence of 40 %wt SDC (0.83, 0.41 and 0.20 Ω.cm^2 at 700, 750 and 800 °C, respectively). In that work, the EIS data of NiO-YSZ/YSZ/SFM-SDC cell was fitted in a $LR_\Omega(Q_HR_H)(Q_LR_L)$ equivalent circuit. It was proposed that addition of SDC reduces the size of high and low-frequency arcs due to the extension of triple phase boundaries (TPBs) and facilitation of surface diffusion and

* Corresponding authors.
E-mail addresses: alireza.babaei@ut.ac.ir (A. Babaei), hamidabdoli@yahoo.com (H. Abdoli).

https://doi.org/10.1016/j.jelechem.2023.117376
Received 8 January 2023; Received in revised form 17 March 2023; Accepted 21 March 2023
Available online 23 March 2023

adsorption, respectively [13]. Despite the results of these studies, the electrochemical behavior of SFM/GDC composite cathode and the limiting steps during ORR still require more investigations.

It has been shown that electrode surface decoration is an effective method to enhance the electrodes' electrochemical activity [15]. In the case of SFM and SFM-based electrodes, the effect of different nano-catalyst infiltration were studied by various authors [12,16]. Xu et al. [17] comprehensively studied the effect of Ni nanoparticles infiltration into the SFM fuel electrode. Yu et al. [18] investigated the SFM-SDC fuel electrode and reported that introduction of Ru to the electrode backbone, improved the electro-catalytic properties of the electrode and reduced the polarization resistance from 0.67 to 0.22 $\Omega.cm^2$ at 3 % H_2O humidified hydrogen. Also, Liu et al. [19] illustrated the effect of Ru impregnation on the SFM-SDC performance toward steam electrolysis with the assistance of partial oxidation of methane (POM). Osinkin et al. [20] used Pr_6O_{11} to promote the SFM/SDC (90/10 wt%) composite cathode performance and observed a 5 to 7 times reduction of electrode polarization resistance due to the facilitation effect of Pr_6O_{11} on oxygen surface exchange. In another research, Zhang et al. [21] indicated that the introduction of SDC nanoparticles into the SFM reduces the electrode polarization resistance due to the increase in surface exchange coefficient by about 100 times [12]. These findings revealed that SFM-based cathodes suffer from insufficient surface exchange reaction rate during ORR. On the other hand, precious metals such as Pd and Ag, were utilized to enhance the electrocatalytic activity of electrodes, since they facilitate surface exchange reaction especially at lower temperature [22,23]. It was reported that impregnation of Pd nanoparticles into Strontium doped Lanthanum Manganite (LSM), LSM/Yttria-stabilized Zirconia (LSM/YSZ) composite, and Lanthanum Strontium Cobalt Ferrite (LSCF) cathodes resulted in a reduction of activation energy of ORR and polarization resistance [24], due to the formation of Pd, PdO, or PdO_x and facilitation of surface reaction and diffusion of oxygen species within the electrode materials [22]. Accordingly, to understand whether an SOFC cathode material is limited by the low surface exchange kinetics, Pd incorporation into the electrode scaffold could also be exploited.

In this report, by aiming electrochemical characterization of the SFM/GDC composite electrode, first the SFM/GDC electrode is symmetrically investigated by the EIS analysis to determine the optimal sintering temperature of the composite cathode. Afterwards, the effect of operational temperature on the EIS response is obtained, and by using the distribution of relaxation times (DRT) analysis, the EIS curves are fitted to an equivalent circuit. The EIS measurements reveal a substantial decrease in the polarization resistance, specifically at lower temperature, after incorporation of Pd nanoparticles into the electrode backbone. Moreover, the resulting EIS and DRT analysis of the Pd impregnated symmetric electrodes would provide a means to directly observe the limitations of bare electrode during ORR; therefore, the utilization criteria of the SFM/GDC electrode would be discerned more profoundly.

2. Materials and methods

2.1. Synthesis

Synthesis of the $Sr_2Fe_{1.5}Mo_{0.5}O_{6-\delta}$ powder was carried out via the sol–gel combustion method as is explained before [25]. Within this procedure, $Sr(NO_3)_2$, $Fe(NO_3)_3{\cdot}9H_2O$, and $(NH_4)_6Mo_7O_{24}{\cdot}4H_2O$ were dissolved in 100 ml of deionized water and then citric acid was added to the solution as the combustion agent. The molar ratio of citric acid to metallic ions was 1.5:1. The solution was stirred at 70 °C for 2 h to form a homogenous solution. For the sake of sol preparation, the pH was fixed at 3 by adding ammonia solution and then the sol was kept at 90 °C until a sticky gel was obtained. In the next step, it was combusted to achieve a solid black foam (ash) by heating in a box oven at 300 °C in air. The obtained ash was ground in an agate mortar and calcined at 1100 °C for 5 h to produce the SFM powder.

2.2. Cell fabrication

SFM/GDC composite powder was prepared by milling the synthesized SFM and $Ce_{0.9}Gd_{0.1}O_{1.95}$ (GDC, Fuel Cell Materials Co.) powders in the ethanol media (with a ratio of 50:50 by weight) for 24 h. The composite powder was dried in an oven at 80 °C for 4 h, and then ground in an agate mortar. The electrolytes pellets were prepared by die pressing of a mixture of 8 mol% Y_2O_3-stabilized ZrO_2 (YSZ, Tosoh, Japan) and 2 wt% polyvinyl butyral (Kuraray) at 70 MPa, followed by sintering at 1500 °C for 4 h. The electrolyte pellets' final diameter and thickness were 20 and 1 mm, respectively. To assemble a symmetrical configuration of SFM/GDC|GDC|YSZ|GDC|SFM/GDC, a GDC ink was prepared, and screen printed on both sides of the YSZ electrolyte to mitigate undesirable reactions between electrode and electrolyte, followed by sintering at 1250 °C for 2 h having a final thickness of 4 μm and an area of 1 cm^2. To prepare the electrode paste, the SFM/GDC composite powder was dispersed in an organic vehicle and roll milled for 24 h to obtain a homogenous mixture. The paste was painted on both sides of the electrolyte with an area of 0.5 cm^2 and sintered at 1000–1150 °C for 2 h in air.

A 0.5 M $Pd(NO)_3$ solution was prepared and infiltrated into the SFM/GDC electrodes up to 4 times, denoted as nD-infiltrated SFM/GDC (n = the number of infiltration sequences). For each infiltration sequence, one droplet was dropped on both sides of the cells, dried at room temperature, followed by calcination at 800 °C for 1 h.

2.3. Characterization

X-ray diffraction was utilized to characterize the synthesized SFM using a Philips 1730-PW X-ray diffractometer with CuKα radiation. Furthermore, symmetrical cell performances were characterized by EIS at open-circuit voltage (OCV) with a Metrohm Autolab potentiostat (PGSTAT302 N, Autolab) in the frequency range of 100 kHz to 0.1 Hz with the AC voltage amplitude of 10 mV in the temperature range of 650 to 800 °C. In order to elaborate the electrode process reactions, the EIS data were fitted in equivalent circuit models (ECM) using ZsimpWin software. The EIS curves were also analyzed by distribution of relaxation times (DRT) using the Tikhonov regularization by DRTtools software to validate and understand the reaction mechanisms.

Microstructural inspections were carried out using a field emission scanning electron microscope (FE-SEM, Tescan) equipped with energy dispersive spectroscopy (EDS).

3. Result and discussion

3.1. Materials characterization and electrode preparation

SFM powder was achieved after calcination at 1100 °C for 5 h. The micrograph of the calcined powder is shown in Fig. 1-a, demonstrating an irregular morphology with the average particle size of ~1 μm. Due to high-temperature calcination, SFM particles were locally connected by neck formation. X-ray diffraction (XRD) pattern of Fig. 1-b demonstrated presence of perovskite peaks corresponding to the reference card no.: 96–153-1826. The obtained pattern is in good agreement with those reported in prior studies [7,13,26]. This proves the formation of cubic $Sr_2Fe_{1.5}Mo_{0.5}O_{6-\delta}$ (SFM) with no sign of any undesirable phase such as $SrMoO_4$.

Fig. 2 demonstrates the obtained EIS spectra of the prepared cells with a symmetrical configuration of SFM/GDC|GDC|YSZ|GDC|SFM/GDC at the testing temperature of 800 °C. For better visualization of the impedance spectra, the inductive tails were removed from the high frequency (HF) part and the ohmic resistances were eliminated by

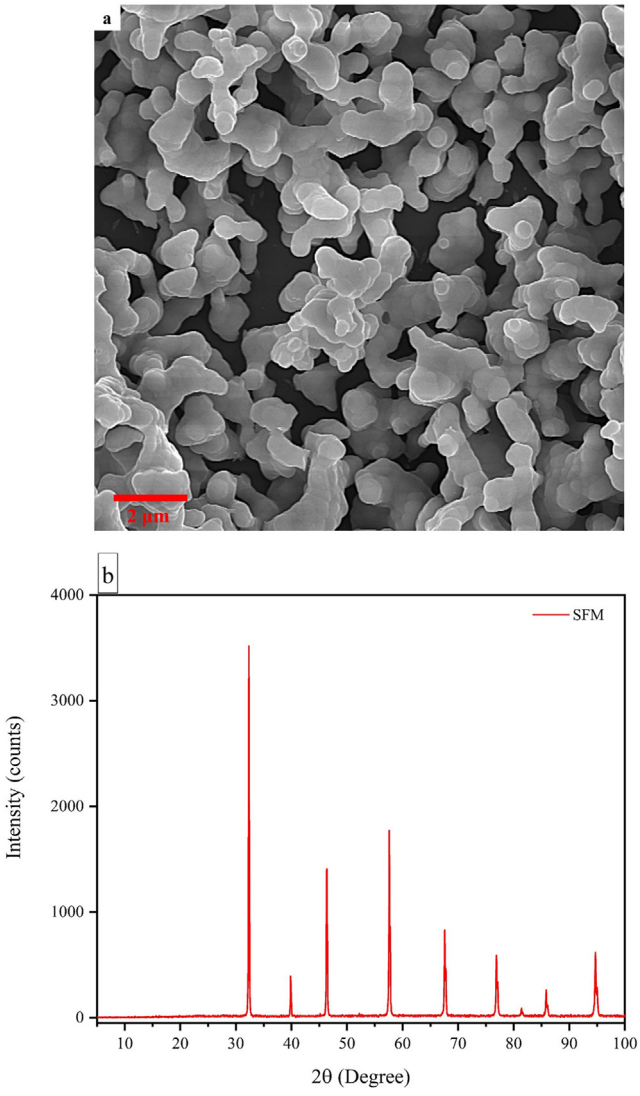

Fig. 1. (a) FESEM micrograph and (b) XRD pattern of $Sr_2Fe_{1.5}Mo_{0.5}O_{6-\delta}$ calcined at 1100 ˚C for 5 h.

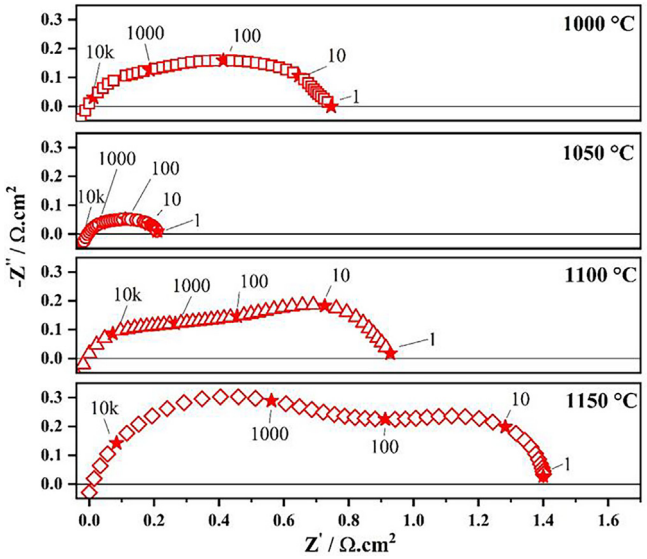

Fig. 2. EIS spectra of SFM/GDC electrodes sintered at different temperature and tested at 800 ˚C (Numbers assigned with star symbols represent frequencies).

shifting the Nyquist curves to zero. The lowest electrode polarization resistance (0.23 Ω.cm^2) was obtained for the electrode sintered at 1050 ˚C.

Fig. 3 (a to d) depicts the cross-section microstructure of the composite electrode sintered at various temperatures corresponding to the EIS responses presented in Fig. 2. Generally, it is known that fine grain sizes, large surface area, good grain interconnection, adequate porosity and good interfacial adhesion between the electrolyte and electrode layers are crucial to obtain high electrode performance. Although the latter is obtained when firing temperature is high enough, sintering at elevated temperature may lead to grain size enlargement or detrimental interactions, both result in high polarization resistance [27]. As it can be seen, the necking between particles and the interfacial bonding between electrode and GDC layer are inadequate after sintering at 1000 ˚C (Fig. 3-a). According to Fig. 2, the polarization resistance of this electrode is about 0.8 Ω.cm^2 which is higher than 0.23 Ω.cm^2 corresponding to the electrode sintered at 1050 ˚C. Fig. 3-b demonstrates the microstructure of SFM/GDC composite electrode sintered at 1050 ˚C in which necked particles, interconnected porosities and good interfacial bonding are obvious with no sign of micro-crack throughout the electrode and the lowest polarization resistance was obtained for this sintering temperature. Sintering at higher temperatures (i.e. 1100 and 1150 ˚C) yields to the higher polarization resistance of the electrode. The increased HF resistance of the EIS spectra is probably associated with the unwanted reaction between electrode and the electrolyte that negatively affects the charge transfer sub-process [28,29]. Morphological studies of the electrodes sintered at 1100 and 1150 ˚C (Fig. 3-c and -d, respectively) shows the increased particle size and the decreased amount of open pores in comparison with those sintered at 1000 and 1050 ˚C (Fig. 3-a and 3-b, respectively). This will cause a slower oxygen gas diffusion through the electrode and a decreased number of active sites for the electrochemical reactions, which ultimately causes a higher resistance at the low frequency (LF) section of the EIS spectra [17 18]. For the electrode sintered at 1100 ˚C (Fig. 3-e), however, a dense interphase layer beneath the GDC barrier layer was found, which is also proved by EDS map analysis (Fig. 3-f), implying the formation of a thin (~0.5 μm) and continuous Sr-rich layer along electrode/electrolyte interface. GDC barrier layer is normally applied on the electrolyte surface to mitigate the reaction between the electrolyte and segregated Sr from the electrode; nonetheless, high temperature sintering would encourage the segregation process and the SrO species motion within the barrier layer [30,31]. The segregated Sr may react with Zr-based electrolytes at high sintering temperature to form $SrZrO_3$ (SZO), which is an undesired phase in SOCs due to its low ionic conductivity and high electronic resistivity [32–34].

3.2. Electrochemical behavior of SFM/GDC cathode

Fig. 4-a depicts the EIS spectra of the SFM/GDC electrode sintered at 1050 ˚C. The electrode polarization resistance is decreased from 1.63 to 0.23 Ω.cm^2 with increasing the testing temperature from 650 to 800 ˚C. This reduction is due to the facilitation of some temperature-dependent ORR sub-processes. The magnitude of polarization resistances is comparable to the previous studies of the SFM-based composite cathodes. As a case in point, Dai et. al [13] reported that the polarization resistance of the SFM-SDC (1:1) composite cathode decreased from 1.58 to 0.21 Ω.cm^2 when the temperature elevates from 650 to 800 ˚C. Moreover, Guo et. al [14] stated the polarization resistance of 2.70 Ω.cm^2 at 650 ˚C for the SFM/GDC (70 wt%:30 wt%) composite electrode utilized in YSZ-supported reversible solid oxide cell.

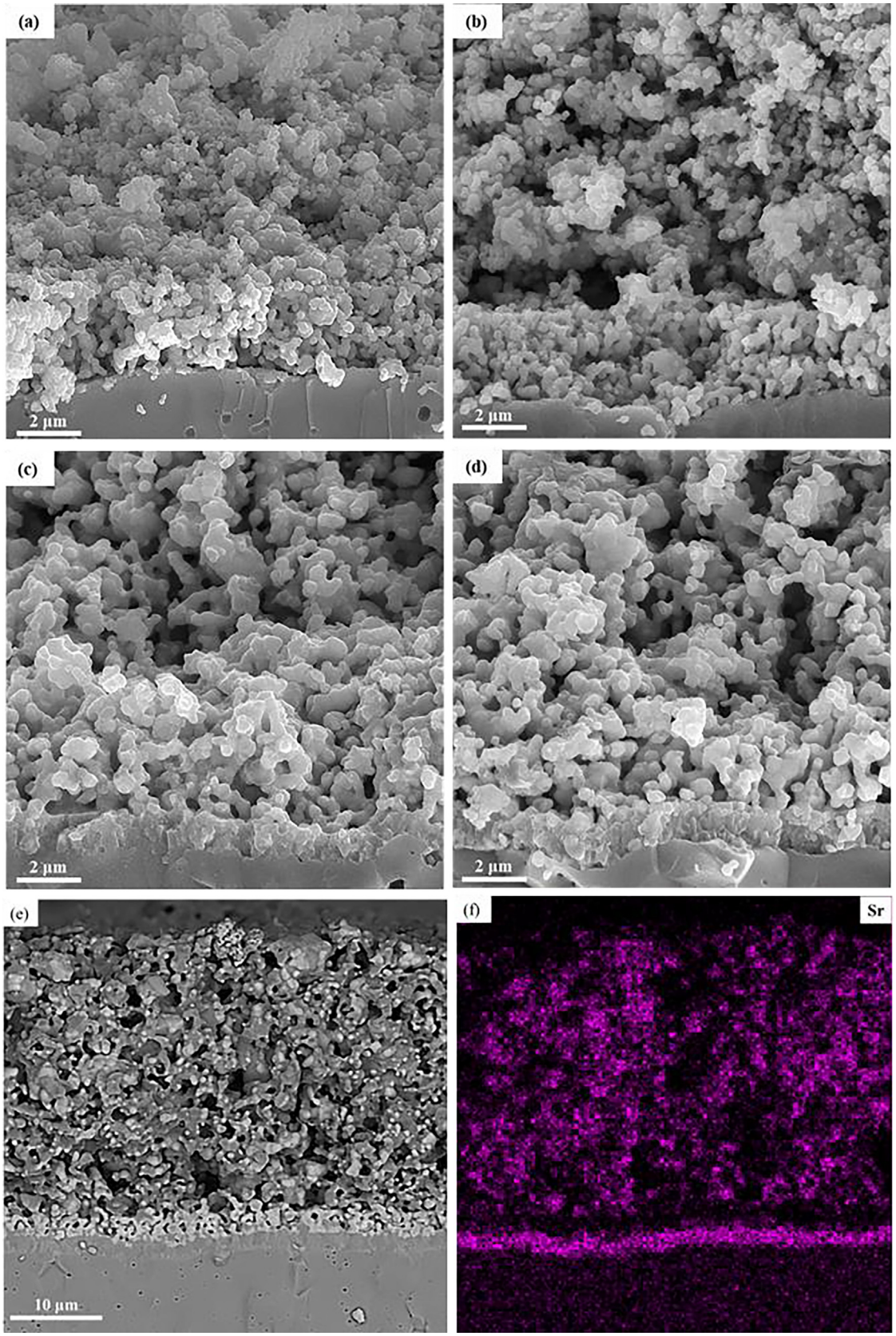

Fig. 3. FESEM images of fractured cross-section of composite electrode sintered at (a) 1000, (b) 1050, (c) 1100, and (d) 1150 °C. (e) backscattered image and (f) EDS selective map for Sr element for the electrode sintered at 1100 °C.

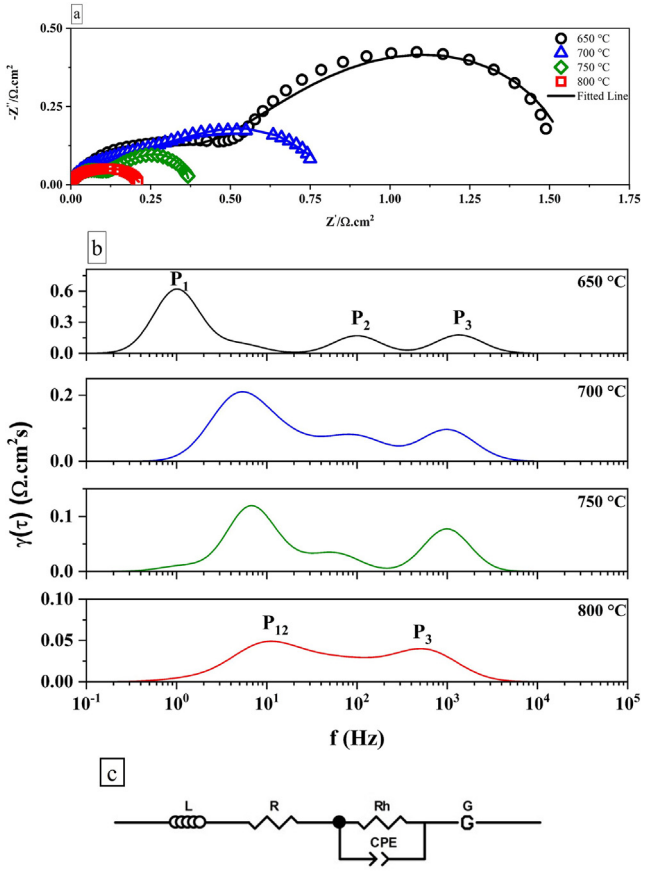

Fig. 4. (a) EIS plots, (b) DRT curves corresponding to the EIS spectra of SFM/GDC electrode sintered at 1050 °C and tested at 650 to 800 °C, and (c) the equivalent circuit.

Analysis of the distribution of relaxation times (DRT) and simulation of EIS data by complex non-linear least square (CNLS) fitting were utilized to get insights into the potential physiochemical reactions that took place in this temperature range (Fig. 4-b and -c). Three DRT peaks (P_1, P_2, and P_3) were identified from EIS data at the testing temperature of 650 °C, indicating that at least three sub-processes contribute to the oxygen reduction reactions. P_1, P_2, and P_3 took place at approximately 1, 100, and 2000 Hz, respectively. Since DRT analysis showed three main peaks, the data seems to be adopted in an equivalent circuit with three RQ elements in series. However, impedance spectra in Fig. 4-a did not lead to a satisfactory fit by an equivalent circuit containing three RQs. Then, using a Gerischer element G, an equivalent circuit of LR(R_HQ)G, presented in Fig. 4-c, was exploited to fit the impedance spectrum, similar to those suggested by other groups [35–39]. For example, Nielsen and co-workers simulated the EIS of LSCF-GDC cathode with a Gerischer element in series with a Finite-Length-Warburg (FLW), demonstrating the co-occurrence of diffusion and oxygen surface exchange reaction in ORR [37]. Adler et al. [40] explained for $La_{0.6}(Ca,Sr)_{0.4}Fe_{0.8}Co_{0.2}O_{3-\delta}$ mixed conductor that a Gerischer element could describe the competition among dissociative adsorption of oxygen and bulk diffusion of oxygen ions. An $R_s(R_1Q)$ G equivalent circuit was proposed for the composite electrodes containing an MIEC and GDC [41–43]. Hjalmarsson and Mogensen [41] applied this model for $La_{0.99}Co_{0.4}Ni_{0.6}O_{3-\delta}$-GDC composite cathode. Also, Khandale et al. [42,43] utilized this model to determine the EIS response of GDC impregnated $Nd_{1.8}Ce_{0.2}CuO_{4+\delta}$ and $Nd_{1.8}Sr_{0.2}NiO_{4-\delta}$-GDC composite cathodes. In the high frequency region of the DRT plot of Fig. 4-b, the characteristic frequency of P_3 is 2000 Hz, so, that peak could be attributed to the charge transfer process at the electrode/electrolyte interface [44]. P_1 and P_2 peaks were found to be described by a Gerischer element very well, as mentioned by Ref. [39]. Therefore, a ZARC element (RQ – a resistant parallel to a constant phase element) associated with charge transfer was proposed for HF part of the spectra. Also, a Gerischer element related to diffusion and surface exchange sub-processes was considered as the LF section of the EIS response. The values obtained from the equivalent circuit model at different temperature are listed in Table 1. R_G and R_H are associated with the resistance of the Gerischer element and the charge transfer resistance, respectively. R_G and R_H decreased respectively by ~91 % and 75 % with temperature rising from 650 to 800 °C. For all temperature, R_G was higher than R_H, but the difference between R_G and R_H was reduced by increasing the temperature. Besides, the height of P_1 and P_2 in the DRT plot (Fig. 4-b), i.e., Gerischer element peaks are decreased by increasing the temperature and they merged into one peak (P_{12}) at 800 °C. This is likely due to thermal activation of the oxygen diffusion and surface exchange processes at high temperature.

According to Khandale et.al. [43], a single Gerischer impedance (Z_G) response can be expressed by:

$$Z_G = \frac{1}{Y_0\sqrt{K_A + i\omega}} = \frac{R_G}{\sqrt{1 + i\omega R_G C_G}} \quad (1)$$

where Y_0 and K_A are the admittance and rate constant, respectively.

Capacitance values corresponding to Gerischer, C_G, demonstrate the dominant path for the diffusion of O^{2-}. Gerischer capacitance lower than 10^{-3} F.cm^{-2} is more readily related to the occurrence of oxygen diffusion along the surface path. Nevertheless, diffusion occurs mainly through the bulk when this value increases to a magnitude of 1 F.cm^{-2} [41–43]. The C_G value estimated from Eq. (1) and its magnitudes were approximately 10^{-1} F.cm^{-2} at all testing temperature. Therefore, it can be concluded that the oxygen ions in SFM/GDC composite electrode were mainly intended to transport through the bulk.

3.3. Effects of electrode surface nano-decoration

Fig. 5 shows the impact of Pd infiltration on the SFM/GDC air electrode polarization resistance at all testing temperatures. The electrode with 3D-Pd solution infiltration has the lowest polarization resistance among all testing temperatures. Thanks to the palladium's high reactivity with oxygen [45], Pd impregnation is assumed to be an effective solution for facilitating the oxygen surface exchange process in ORR.

Through EIS assessments of the infiltrated electrodes at 650–800 °C, the effect of Pd nanoparticles on ORR was investigated by calculating the activation energy (E_a), i.e., plotting ln(R_p) vs. 1/T. Fig. 6 illustrates the Arrhenius plots for the total polarization resistance of the electrode with different Pd loadings. While infiltration of one droplet Pd into the SFM/GDC electrode reduced the E_a by ~10%, slight changes in E_a was observed with higher Pd loadings. The lowest activation energy of 0.98 eV was calculated for the sample with infiltration of 3 droplets. Microstructure of this electrode shows that Pd nanoparticles are well distributed along the interior region of composite electrode (Fig. 7). EDS spectra collected from different points (shown in Fig. 7-a and Table 2) confirmed the presence of Pd nanoparticles on the composite electrode.

Fig. 8 compares the impedance responses of the SFM/GDC-based electrode with various infiltration sequences at two temperature of 650 °C (Fig. 8-a) and 800 °C (Fig. 8-b). The EIS spectra in Fig. 8 were fitted by a similar EC to that of composite electrode (Fig. 4-c). Analyzing the fitting results at 650 °C shows that adding Pd to the composite electrode, significantly changes R_G compared to R_H. Infiltrating 3 droplets of Pd solution into the composite electrode reduces R_G and R_H at 650 °C by ~48% and ~27%, respectively. However, by incorporating the same amount of Pd at 800 °C, R_G and R_H decreases 10% and 38%, respectively. This implies that the influence of Pd incorporation on the Gerischer resistance was more drastic at lower temperature.

Table 1
Impedance parameters resulted from fitting equivalent circuit at different temperatures.

T (°C)	R_H (Ω.cm^2)	R_G (Ω.cm^2)	Y_0 (S.sec$^{0.5}$)	K_A (sec^{-1})
650	0.52	1.15	0.47	3.40
700	0.33	0.45	0.55	16.50
750	0.16	0.26	0.74	25.50
800	0.13	0.10	1.03	92.78

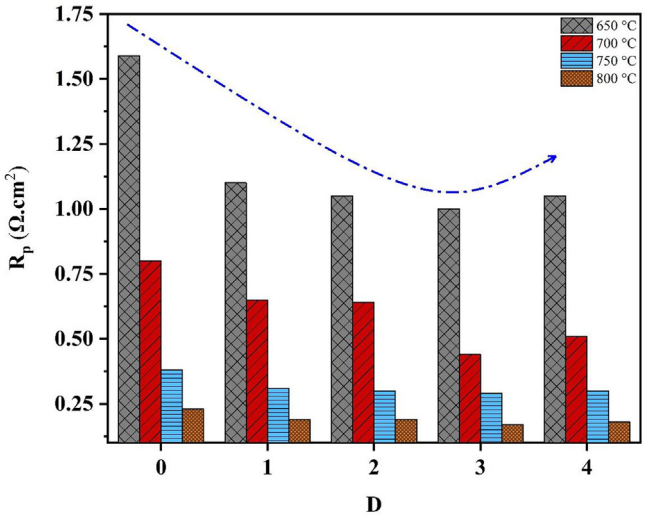

Fig. 5. Polarization resistance of the SFM/GDC electrodes vs. different Pd infiltration sequence (D = 0–4) at 650 to 800 °C under OCV.

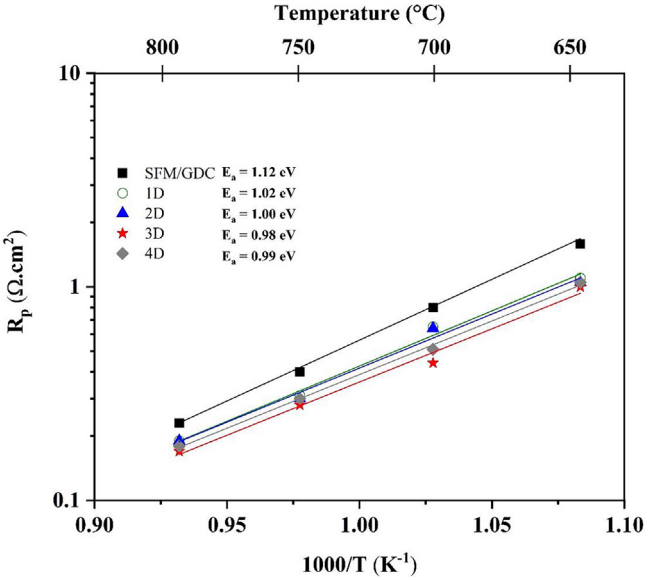

Fig. 6. Arrhenius plots for SFM/GDC electrodes with different Pd infiltration sequence under OCV.

Meanwhile, impregnating Pd does not change the C_G value and it was still around 10^{-1} F.cm^{-2} at all the examined temperatures. The diffusion route of the oxygen ions through the electrode, therefore, are not likely to change by Pd infiltration, and bulk diffusion has remained the dominant diffusion path. Revealed by these observations, the nanosurface decoration on this electrode could only be valuable at intermediate temperature, while this electrode shows reasonable electrocatalytic activity at high working temperature.

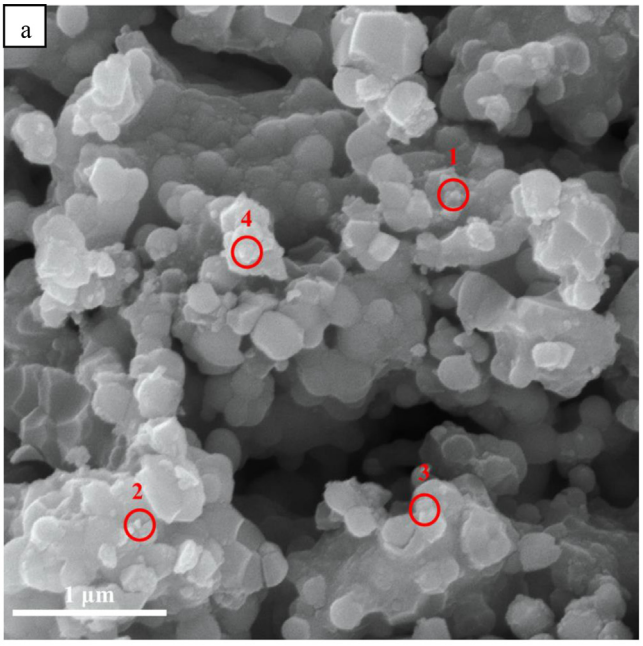

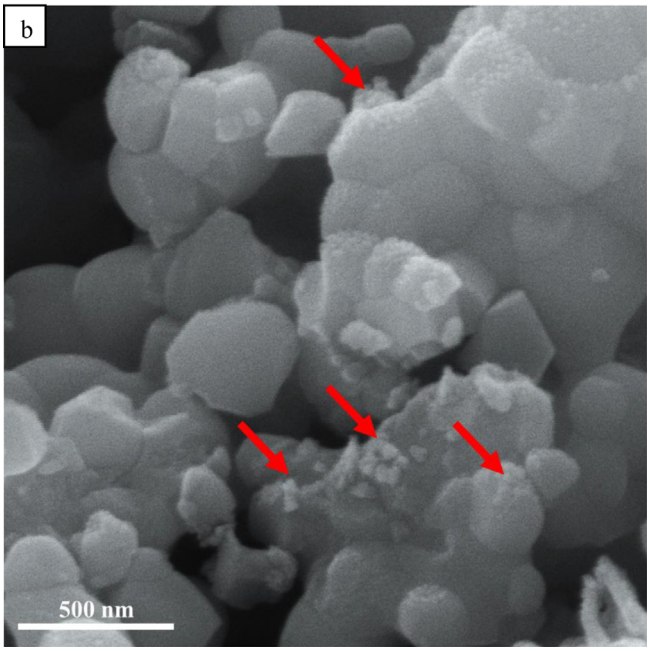

Fig. 7. FESEM image of interior zone of composite electrode infiltrated 3 times by Pd solution at (a) 50.0 kx and (b) 100.0 kx. EDS spectra were collected from points 1 to 4.

For better elucidation of the limiting sub-processes involved in the Gerischer response by means of Pd impregnation, DRT plots of the SFM/GDC and 3D-Pd infiltrated SFM/GDC electrode at 650 °C are presented in Fig. 9. This figure suggests that the presence of Pd in the SFM/GDC backbone led to shift the DRT peaks toward medium frequencies in comparison to the DRT response of bare electrode. Additionally, incorporation of Pd nanoparticles affected P_1 more than the other peaks. Therefore, since impregnation of 3D-Pd solution to the composite electrode resulted in lower R_G, most of its' reduction must be allocated to impregnation effect on the process associated with P_1 peak. Hence, P_1 should be related to oxygen surface reaction because

Table 2
Relative intensity analysis of EDS spectra for points 1 to 4 indicated in Fig. 7-a.

Elements	Point 1 (%)	Point 2 (%)	Point 3 (%)	Point 4 (%)
O	18.34	15.60	22.40	14.17
Fe	9.04	10.00	7.20	9.32
Sr	13.81	14.69	12.80	12.60
Mo	8.68	9.20	9.81	9.70
Pd	6.86	6.91	7.04	7.40
Ce	36.45	36.83	34.65	39.23
Gd	6.82	6.78	6.10	7.59
Total	100	100	100	100

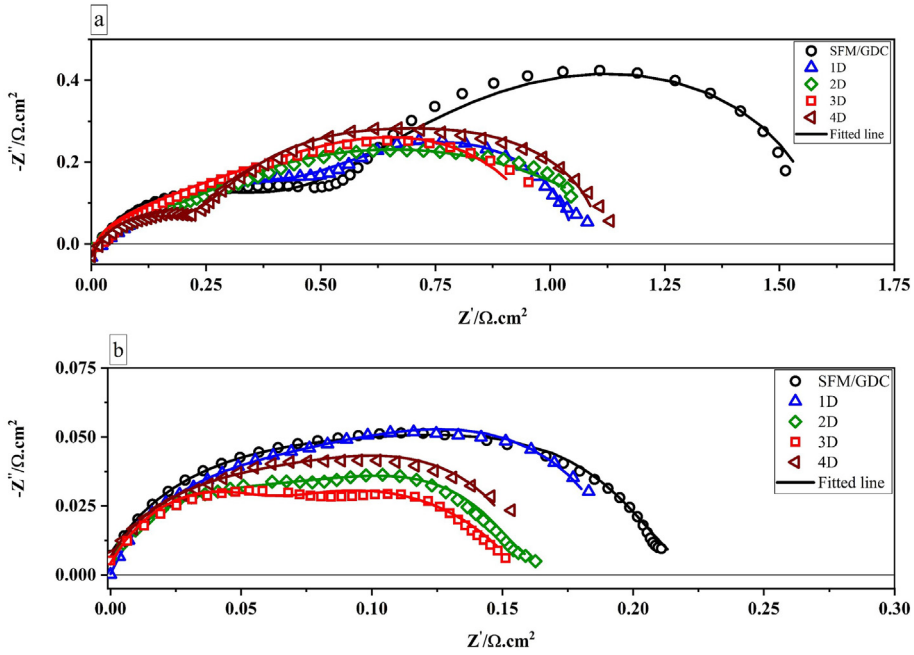

Fig. 8. Nyquist plots for the SFM/GDC electrodes with different Pd infiltration under OCV at (a) 650 °C and (b) 800 °C.

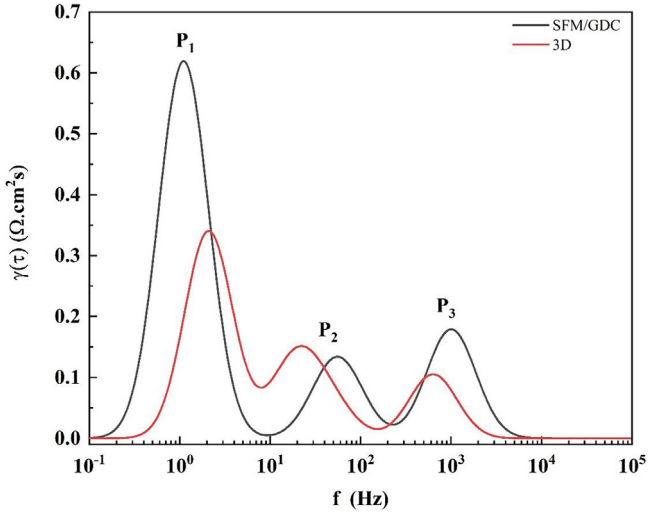

Fig. 9. DRT curves for 3D-Pd infiltrated and bare SFM/GDC electrode at 650 °C.

of the dominant effect of Pd on this process. As a result, P_2 must be accompanied with diffusion, and based on the C_G consistency after surface decoration, diffusion path must not have altered by Pd addition. It is also worth mentioning that P_3 has shown a minor reduction by Pd infiltration. However, the effect of Pd on charge transfer at the electrode/electrolyte interface has not been investigated yet.

4. Conclusion

In this study, electrochemical behavior of SFM/GDC electrode and the effects of Pd infiltration onto the composite cathode were investigated by means of EIS and DRT. To reach this goal, $Sr_2Fe_{1.5}Mo_{0.5}O_{6-\delta}$ (SFM) was synthesized and mixed with $Gd_{0.1}Ce_{0.9}O_{1.95}$ (GDC) to make a composite cathode. The electrode sintered at 1050 °C showed the lowest polarization resistance of 0.23 Ω.cm^2 at 800 °C. DRT analysis indicates three different peaks with distinctive characteristic frequencies at 650 °C, which led to consistent $LR_\Omega(R_HQ)G$ equivalent circuit fit. This equivalent circuit suggests that the charge transfer process corresponds to the high-frequency part of the EIS spectra and a Gerischer impedance response at low frequencies is related to the co-participation of oxygen diffusion and surface exchange, corresponding to two lower frequency peaks in DRT plot. Increasing the testing temperature from 650 to 800 °C reduces the polarization resistance by lowering R_H and R_G by ~75% and ~91%, respectively. This reduction shows the substantial effect of temperature elevation on the processes associated with Gerischer impedance response. Infiltration of Pd onto the SFM/GDC cathode reduced polarization resistance of the electrode especially at lower testing temperature. Besides, the lowest values of activation energy and polarization resistance of the impregnated electrode occurrs by 3 times Pd infiltration. Pd incorporation reduces R_G

by ~48% and ~10% at 650 and 800 °C, respectively. Hence, the significant effects of Pd incorporation on SFM/GDC composite electrode demonstrate that this electrode requires enhancement through surface modification at intermediate temperature range, while surface decoration does not significantly alter the electrocatalytic activity of the SFM/GDC composite electrode toward ORR at high temperatures.

CRediT authorship contribution statement

Arsalan Zare: Investigation, Visualization, Writing – original draft, Formal analysis. **Hirad Salari:** Investigation, Visualization, Writing – original draft, Formal analysis. **Alireza Babaei:** Conceptualization, Methodology, Writing – review & editing, Supervision, Project administration. **Hamid Abdoli:** Conceptualization, Methodology, Supervision, Project administration, Writing – review & editing. **Hamed Aslannejad:** Conceptualization, Methodology, Writing – review & editing, Supervision.

Declaration of Competing Interest

The authors declare that they have no known competing financial interests or personal relationships that could have appeared to influence the work reported in this paper.

References

[1] J.T. Irvine, P. Connor, Solid oxide fuels cells: facts and figures, Springer, 2013.
[2] H. Ding, Nanostructured electrodes for high-performing solid oxide fuel cells, Nanostructured Materials for Next-Generation Energy Storage and Conversion: Springer, 2018, pp. 227–247.
[3] K. Chen, Materials degradation of solid oxide electrolysis cells, J. Electrochem. Soc. 163 (11) (2016) F3070.
[4] A. Tarancon, M. Burriel, J. Santiso, S.J. Skinner, J.A. Kilner, Advances in layered oxide cathodes for intermediate temperature solid oxide fuel cells, J. Mater. Chem. 20 (19) (2010) 3799–3813.
[5] G. Xiao, Q. Liu, F. Zhao, L. Zhang, C. Xia, F. Chen, Sr2Fe1.5Mo0.5O6 as Cathodes for Intermediate-Temperature Solid Oxide Fuel Cells with La0.8Sr0.2Ga0.87Mg0.13O3 Electrolyte, J. Electrochem. Soc. 158 (5) (2011) B455.
[6] Q. Liu et al, Sr2Fe1. 5Mo0. 5O6− δ as a regenerative anode for solid oxide fuel cells, J. Power Sources 196 (22) (2011) 9148–9153.
[7] Q. Liu, X. Dong, G. Xiao, F. Zhao, F. Chen, A novel electrode material for symmetrical SOFCs, Adv. Mater. 22 (48) (2010) 5478–5482.
[8] M.K. Rath, K.-T. Lee, Superior electrochemical performance of non-precious Co-Ni-Mo alloy catalyst-impregnated Sr2FeMoO6-δ as an electrode material for symmetric solid oxide fuel cells, Electrochim. Acta 212 (2016) 678–685.
[9] G. Xiao, Q. Liu, S. Nuansaeng, F. Chen, Sr2Fe1+ xMo1-xO6-δ as anode materials for solid oxide fuel cells, ECS Trans. 45 (1) (2012) 355–362.
[10] J.H. Wright, A.V. Virkar, Q. Liu, F. Chen, Electrical characterization and water sensitivity of Sr2Fe1. 5Mo0. 5O6− δ as a possible solid oxide fuel cell electrode, J. Power Sources 237 (2013) 13–18.
[11] B. He, L. Zhao, S. Song, T. Liu, F. Chen, C. Xia, Sr 2 Fe 1.5 Mo 0.5 O 6−δ - Sm 0.2 Ce 0.8 O 1.9 Composite Anodes for Intermediate-Temperature Solid Oxide Fuel Cells, J. Electrochem. Soc. 159 (5) (2012) B619–B626.
[12] P. Qiu, S. Sun, J. Li, L. Jia, A review on the application of Sr2Fe1. 5Mo0. 5O6-based oxides in solid oxide electrochemical cells, Sep. Purif. Technol. (2022) 121581.
[13] N. Dai, Z. Lou, Z. Wang, X. Liu, Y. Yan, J. Qiao, T. Jiang, K. Sun, Synthesis and electrochemical characterization of Sr2Fe1. 5Mo0. 5O6–Sm0. 2Ce0. 8O1. 9 composite cathode for intermediate-temperature solid oxide fuel cells, J. Power Sources 243 (2013) 766–772.
[14] Y. Guo et al, Characterization of Sr2Fe1. 5Mo0. 5O6-δ-Gd0. 1Ce0. 9O1. 95 symmetrical electrode for reversible solid oxide cells, Ceram. Int. 45 (8) (2019) 10969–10975.
[15] D. Ding, X. Li, S.Y. Lai, K. Gerdes, M. Liu, Enhancing SOFC cathode performance by surface modification through infiltration, Energ. Environ. Sci. 7 (2) (2014) 552–575.
[16] D.A. Osinkin, A.V. Khodimchuk, N.M. Porotnikova, N.M. Bogdanovich, A.V. Fetisov, M.V. Ananyev, Rate-Determining Steps of Oxygen Surface Exchange Kinetics on Sr2Fe1. 5Mo0. 5O6− δ, Energies 13 (1) (2020) 250.
[17] J. Xu et al, Enhancing performance of molybdenum doped strontium ferrite electrode by surface modification through Ni infiltration, Int. J. Hydrogen Energy 46 (18) (2021) 10876–10891.
[18] W. Yu, D. Zhang, X. Zhang, T. Liu, Y. Wang, Advanced Ru-Infiltrated Perovskite Oxide Electrodes for Boosting the Performance of Syngas Fueled Solid Oxide Fuel Cell, ChemElectroChem 9 (7) (2022) e202200024.
[19] T. Liu et al, A robust solid oxide electrolyzer for highly efficient electrochemical reforming of methane and steam, J. Mater. Chem. A 7 (22) (2019) 13550–13558.
[20] D. Osinkin, S. Beresnev, N. Bogdanovich, Influence of Pr6O11 on oxygen electroreduction kinetics and electrochemical performance of Sr2Fe1. 5Mo0. 5O6-δ based cathode, J. Power Sources 392 (2018) 41–47.
[21] L. Zhang, Y. Liu, Y. Zhang, G. Xiao, F. Chen, C. Xia, Enhancement in surface exchange coefficient and electrochemical performance of Sr2Fe1. 5Mo0. 5O6 electrodes by Ce0. 8Sm0. 2O1. 9 nanoparticles, Electrochem. Commun. 13 (7) (2011) 711–713.
[22] A. Babaei, L. Zhang, E. Liu, Performance and stability of La0. 8Sr0. 2MnO3 cathode promoted with palladium based catalysts in solid oxide fuel cells, J. Alloy. Compd. 509 (14) (2011) 4781–4787.
[23] S.V. Seyed-Vakili, A. Babaei, M. Ataie, S. Heshmati-Manesh, H. Abdizadeh, Enhanced performance of La0. 8Sr0. 2MnO3 cathode for solid oxide fuel cells by co-infiltration of metal and ceramic precursors, J. Alloy. Compd. 737 (2018) 433–441.
[24] S.P. Jiang, Nanoscale and nano-structured electrodes of solid oxide fuel cells by infiltration: advances and challenges, Int. J. Hydrogen Energy 37 (1) (2012) 449–470.
[25] Y.A. Farzin, A. Babaei, T.L. Skafte, E. Stamate, A. Ataie, S.H. Jensen, Low-temperature preparation and investigation of electrochemical properties of SFM/CGO composite electrode, Solid State Ion. 356 (2020) 115435.
[26] Q. Liu, C. Yang, X. Dong, F. Chen, Perovskite Sr2Fe1. 5Mo0. 5O6− δ as electrode materials for symmetrical solid oxide electrolysis cells, Int. J. Hydrogen Energy 35 (19) (2010) 10039–10044.
[27] N. Hildenbrand, B.A. Boukamp, P. Nammensma, D.H. Blank, Improved cathode/electrolyte interface of SOFC, Solid State Ion. 192 (1) (2011) 12–15.
[28] M.J. Jørgensen, M. Mogensen, Impedance of solid oxide fuel cell LSM/YSZ composite cathodes, J. Electrochem. Soc. 148 (5) (2001) A433.
[29] S. Jiang, J. Zhang, K. Foger, Deposition of Chromium Species at Sr-Doped LaMnO3 Electrodes in Solid Oxide Fuel Cells II. Effect on O 2 Reduction Reaction, J. Electrochem. Soc. 147 (9) (2000) 3195.
[30] J.S. Hardy, J.W. Templeton, D.J. Edwards, Z. Lu, J.W. Stevenson, Lattice expansion of LSCF-6428 cathodes measured by in situ XRD during SOFC operation, J. Power Sources 198 (2012) 76–82.
[31] F. Wang, M. Nishi, M.E. Brito, H. Kishimoto, K. Yamaji, H. Yokokawa, T. Horita, Sr and Zr diffusion in LSCF/10GDC/8YSZ triplets for solid oxide fuel cells (SOFCs), J. Power Sources 258 (2014) 281–289.
[32] F.W. Poulsen, N. van der Puil, Phase relations and conductivity of Sr-and La-zirconates, Solid State Ion. 53 (1992) 777–783.
[33] F. Wankmüller, J. Szász, J. Joos, V. Wilde, H. Störmer, D. Gerthsen, E. Ivers-Tiffée, Correlative tomography at the cathode/electrolyte interfaces of solid oxide fuel cells, J. Power Sources 360 (2017) 399–408.
[34] T. Matsuda, S. Yamanaka, K. Kurosaki, S.-I. Kobayashi, High temperature phase transitions of SrZrO3, J. Alloy. Compd. 351 (1–2) (2003) 43–46.
[35] A. Flura, C. Nicollet, V. Vibhu, B. Zeimetz, A. Rougier, J.-M. Bassat, J.-C. Grenier, Application of the Adler-Lane-Steele model to porous La2NiO4+ δ SOFC cathode: influence of interfaces with gadolinia doped ceria, J. Electrochem. Soc. 163 (6) (2016) F523–F532.
[36] P. Costamagna, E.M. Sala, W. Zhang, M.L. Traulsen, P. Holtappels, Electrochemical impedance spectroscopy of La0. 6Sr0. 4Co0. 2Fe0. 8O3-δ nanofiber cathodes for intermediate temperature-solid oxide fuel cell applications: a case study for the 'depressed'or 'fractal'Gerischer element, Electrochim. Acta 319 (2019) 657–671.
[37] J. Nielsen, T. Jacobsen, M. Wandel, Impedance of porous IT-SOFC LSCF: CGO composite cathodes, Electrochim. Acta 56 (23) (2011) 7963–7974.
[38] J. Nielsen, J. Hjelm, Impedance of SOFC electrodes: a review and a comprehensive case study on the impedance of LSM: YSZ cathodes, Electrochim. Acta 115 (2014) 31–45.
[39] B.A. Boukamp, A. Rolle, Use of a distribution function of relaxation times (DFRT) in impedance analysis of SOFC electrodes, Solid State Ion. 314 (2018) 103–111.
[40] S.B. Adler, J.A. Lane, B.C.H. Steele, Electrode kinetics of porous mixed-conducting oxygen electrodes, J. Electrochem. Soc. 143 (11) (1996) 3554–3564.
[41] P. Hjalmarsson, M. Mogensen, La0. 99Co0. 4Ni0. 6O3− δ–Ce0. 8Gd0. 2O1. 95 as composite cathode for solid oxide fuel cells, J. Power Sources 196 (17) (2011) 7237–7244.
[42] A. Khandale, S. Bhoga, Nd1. 8Ce0. 2CuO4+ δ: Ce0. 9Gd0. 1O2− δ as a composite cathode for intermediate-temperature solid oxide fuel cells, J. Power Sources 268 (2014) 794–803.
[43] A. Khandale, R. Lajurkar, S. Bhoga, Nd1. 8Sr0. 2NiO4− δ: Ce0. 9Gd0. 1O2− δ composite cathode for intermediate temperature solid oxide fuel cells, Int. J. Hydrogen Energy 39 (33) (2014) 19039–19050.
[44] M. Ghamarinia, A. Babaei, C. Zamani, Electrochemical characterization of La2NiO4-infiltrated La0. 6Sr0. 4Co0. 2Fe0. 8O3-δ by analysis of distribution of relaxation times, Electrochim. Acta 353 (2020) 136520.
[45] S. Wang, H. Zhong, High performance Pd promoted Sm0. 5Sr0. 5CoO3–La0. 8Sr0. 2Ga0. 8Mg0. 15Co0. 05O3− δ composite cathodes for intermediate temperature solid oxide fuel cells, J. Power Sources 165 (1) (2007) 58–64.